Int J Adv Manuf Technol (2017) 93:3693–3703
DOI 10.1007/s00170-017-0436-5

ORIGINAL ARTICLE

Closed-loop quality control system for laser chemical machining in metal micro-production

P. Zhang[1] · **A. von Freyberg**[1] · **A. Fischer**[1]

Received: 12 December 2016 / Accepted: 18 April 2017 / Published online: 25 July 2017

Abstract Small geometrical features in the scale of 10 to 400 μm can be produced on metallic workpieces with the laser-induced chemical etching process at low costs. However, the interactions among the subsystems of the laser chemical etching process, the mechanical positioning unit, the etchant pump, the laser source, and among the removal paths hinder the precise determination of the required process parameters for producing the desired geometry. For this reason, a closed-loop quality control is designed to compensate the deviations of quality features of a single removal and also of a workpiece produced by a sequence of removals. The developed control approach is based on inverse process models, which are used for a feed-forward control. Finally, a closed-loop control is achieved by designing an adaptive controller for the non-linear multi-inputs-multi-outputs process. The closed-loop control is realized as a production-discrete control by using a post-production measurement, and applied for producing a micro forming tool in the shape of a rectangular die. As a result, the laser chemical etching process is stabilized and, thus, the desired geometrical quality features of the workpiece are obtained with a reduced shape deviation of 2.4 μm.

Keywords Quality control · Micro-production · Model predictive control · Adaptive control

✉ A. von Freyberg
a.freyberg@bimaq.de

[1] University of Bremen, Bremen Institute for Metrology, Automation and Quality Science (BIMAQ), Linzer Str. 13, 28359 Bremen, Germany

1 Introduction

The laser-induced chemical etching process also known as laser chemical machining (LCM) is a new method for micro-finishing of metals with high hardness. In this process, a focused laser beam heats up the surface of the workpiece and activates a local material removal by chemical reactions [1]. With a sequence of overlapping removals, a desired complex geometry can be produced in principle.

Due to a non-contact production without expensive special tools, the production costs using LCM are lower than those of other methods, e.g., micro-milling [2] and micro-electrical discharge machining (μEDM) [3]. The lump sum price for laboratory LCM amounts to about 20 EUR/hour. Furthermore, LCM combines advantages of laser ablation and electrochemical machining (ECM). The removal by dint of chemical reaction avoids melting of material, which can be caused by laser ablation, and also achieves a high-quality surface without burrs and debris [4]. Compared to ECM, the LCM realizes a precise localized material removal in the laser-heated areas [5]. The LCM has the potential to achieve a small geometry (between 10 and 400 μm in cross-section) with a roughness of 0.3 μm [6, 12]. However, many pre-experiments are needed to manually determine the optimal process parameters to produce the desired geometry. In order to reduce the costs of pre-experiments and to improve both the process accuracy and stability, a closed-loop quality control has to be designed for the LCM.

1.1 LCM principle

The material removal in LCM is based on the laser-induced thermochemical reactions between the etchant and the metal on the workpiece surface. During processing, hydrogen ions

(H^+) and metal atoms (Me) build up hydrogen (H_2) and water soluble metallic salts (Me^{2+}) [2]:

$$Me + 2H^+ \rightarrow Me^{2+} + H_2. \quad (1)$$

In principle, metals with a specific passivation layer, which protects the workpiece against a chemical dissolution in acid at room temperature, could be machined by this method [4]. An acid, e.g., sulfuric acid, hydrochloric acid, and phosphoric acid with low concentration can be used as etchant for different metals. In this contribution, phosphoric acid (H_3PO_4) with a concentration of 5 mol/l is used for processing the inhomogeneous alloy Stellite 21, which is produced by selective laser melting. This chemical reaction takes place in a laser-heated area at approximately 90 °C [3].

The functional principle of LCM is depicted in Fig. 1. By varying the process input parameters $\boldsymbol{u} = (P \; v \; Q)$, i.e., the laser power P, the feed rate v of the workpiece and the flow rate Q of the etchant, a different removal contour with the shape parameter $\boldsymbol{a}$ is achieved. Here, $\boldsymbol{a} = (a_1 \quad a_2)$ with a_1 and a_2 as a measure of the depth and the width of the removal, respectively. Hence, the process behavior $\boldsymbol{H}_{\mathbf{LCM}}$ is described by

$$\boldsymbol{a} = \boldsymbol{H}_{\mathbf{LCM}}(\boldsymbol{u}). \quad (2)$$

1.2 State of the art and aims of the work

The mechanisms of LCM have already been studied [5, 7, 8]. By analyzing the relation between the etching probability distribution and the estimated laser heating area, the probable removal was described by a Gaussian function [9]. Furthermore, the contour of the removal cavity associated to laser power and material feed rate was modeled with an empirical formula [10], and influences of the etchant flow rate and existing chemical and hydrodynamic disturbances in LCM were described in [11]. Besides the physical analysis of individual process parameters, a process-model based on an artificial neural network (ANN) was introduced, which incorporates all important parameters such as laser power, material feed rate, and etchant flow rate [12]. However, in the process chain of LCM production with multiple removals, the quality of the previous step influences the achievable production quality of the subsequent processing steps [13]. Here, a single removal path can be considered as one process in the LCM process chain. In order to compensate the interactions among the subsequent removals, and also the inaccuracy of the ANN-based process model, a closed-loop quality control is required.

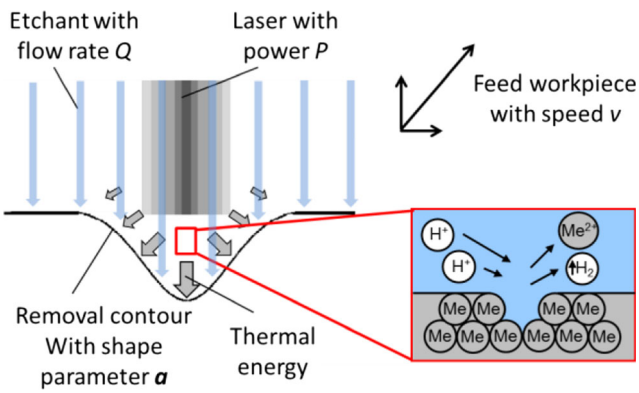

Fig. 1 The functional principle of LCM

For this reason, the design, the validation, and the application of such an LCM quality control are presented in this paper. The main focuses are the improvement of the model accuracy, the realization of a quality feed-forward control, and the design of a suitable controller for the closed-loop control. Note that a production-discrete quality control is designed here, because in situ measurements are still under development. Production-discrete means that the control loop is time discrete and closed by using post-production measurements with a confocal microscope. The aims of the LCM quality control are:

- the control of the achieved geometry of a single removal path (result of a single process),
- the control of the produced workpiece geometry by multiple removals (result of multiple processes).

Therefore, a cross-path control is required for the process chain. This means, the quality of the workpiece is controlled by adjusting the process parameters of multiple superimposing paths under the consideration of cross-linked influences. The general cross-process quality control concept was introduced in [14], and has been successfully applied, e.g., for a bearing ring production process chain [15, 16]. Here, the cross-process control concept is applied for a closed-loop quality control of the LCM. For this purpose, the LCM process identification is discussed and the interactions of multiple paths (processes) are studied. Finally, an adaptive controller is designed for the closed-loop control to cope with the non-linear behavior of the LCM process. As a result, the shape deviations of the produced workpiece from the desired geometry are shown to be distinctly reduced with the developed quality control. For example, the maximal shape deviation of a manufactured rectangular die is reduced from 33.1 μm (without closed-loop control) to 2.4 μm (with closed-loop control) after two production steps.

The experimental setup of LCM is described in Section 2. The approach of the quality control is introduced in Section 3. A detailed derivation and study of the control system, which includes the process model and a simulation of the process chain, follows in Section 4. Finally, the validation of the control system and its application to produce a micro-forming tool are presented in Section 5.

2 Experimental setup

The experimental setup is illustrated schematically in Fig. 2. A workpiece is fixed in an etchant container, which is mounted on a linear stage system with an axis resolution of 0.05 μm (*Newport PM500*), and covered by the etchant. During processing, the workpiece is positioned by the stage. A fiber-laser (*Trumpf TruFiber 300*) with a wavelength of 1080 nm is focused by a telescope system to a diameter of 24 μm. The focused laser goes through an etchant jet nozzle with a diameter of 1.5 mm and heats the material surface. The etchant jet-stream is pumped coaxially to the laser beam, dissolves the metallic material, and at the same time cools the processing area.

For the automation of the LCM-setup in one platform, an industrial computer with the operating system xPC, equipped with a multi-channel serial interface (*RS232*) and an analog-digital converter (*National Instrument PCI-6024E*), is used for the real-time adjustment of the process input parameters. Note that the relation between the laser power and the respective voltage input signal for the laser control is post-process measured, so that the latter can be used for adjusting the laser power during LCM processing.

3 Control aim and challenges

For the LCM production chain, a control of the workpiece quality features is desired, e.g., for the geometry of a rectangular die and the flatness of the produced surface. Considering the geometry $\boldsymbol{G}$ of the workpiece as the result of the superposition of multiple removal paths, a direct control of the workpiece quality features by adjusting all the process input parameters from every removal path is difficult to achieve, because of excessive degrees of freedom and the non-linear process behavior. In order to reduce the degrees of freedom, only the shape parameters $\boldsymbol{a_j}$ of every path $j = 1,\ldots,N_{\text{path}}$ are changed in the control loops, while the set-value of the position parameter remains constant. The combination of the shape parameters from N_{path} paths are summarized as $\boldsymbol{A} = \left(\boldsymbol{a_1}, \cdots, \boldsymbol{a_{\text{Npath}}}\right)^T$. Note that the shape parameters $\boldsymbol{A}$ are the control variables, and the process input parameters $\boldsymbol{U} = \left(\boldsymbol{u_1}, \cdots, \boldsymbol{u_{\text{Npath}}}\right)^T$ of multiple paths are the actuating variables. This control of the process chain can also be considered as a combination of N_{path} control loops for individual processes, i.e., single paths with the control variables $\boldsymbol{a_j}$ and the actuating variables $\boldsymbol{u_j}$. After each production, the measured geometry $\boldsymbol{G_{\text{meas}}}$ of the workpiece is compared to the desired quality features $\boldsymbol{G_{\text{desi}}}$ (post-production measurement and, thus, production-discrete control). If the deviations remain in the defined tolerance range, the set-values of the process parameters are recorded and used for future productions. Otherwise, the deviations are compensated by controlling the shape parameters contained in $\boldsymbol{A}$. The production step number is denoted by i. A schematic flow chart of this quality control is illustrated in Fig. 3.

The developed quality control approach is depicted in Fig. 4. It contains a feed-forward control [17] and consists of the following blocks:

- a path plan for the prediction of the set-value $\boldsymbol{A_{\text{theo}}}$ for all paths in the production chain according to the desired geometry $\boldsymbol{G_{\text{desi}}}$ and the initial geometry $\boldsymbol{G_{\text{init}}}$ of the workpiece;
- an observer to estimate the control variables $\boldsymbol{A_{\text{meas}}}$ from the measured geometry $\boldsymbol{G_{\text{meas}}}$;
- a quality controller to adjust all the shape parameters $\boldsymbol{A}_{\text{adju}}$ for the subsequent production according to the deviation between the set-value $\boldsymbol{A_{\text{theo}}}$ and the measurements $\boldsymbol{A_{\text{meas}}}$;
- an inverse process model as actuating element to calculate the process input parameters $\boldsymbol{U}$ for multiple removal paths according to the adjusted shape parameters $\boldsymbol{A_{\text{adju}}}$;
- a post-process measurement to measure the machined workpiece, which can be considered as a dead time element.

With this production-discrete control loop, the process parameters are continuously optimized for the subsequent

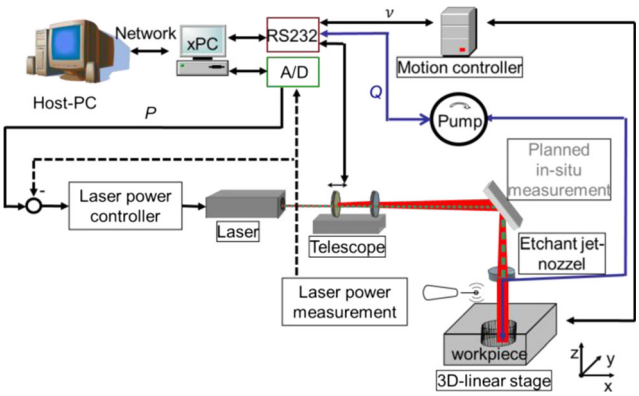

Fig. 2 Experimental setup and automation concept of LCM

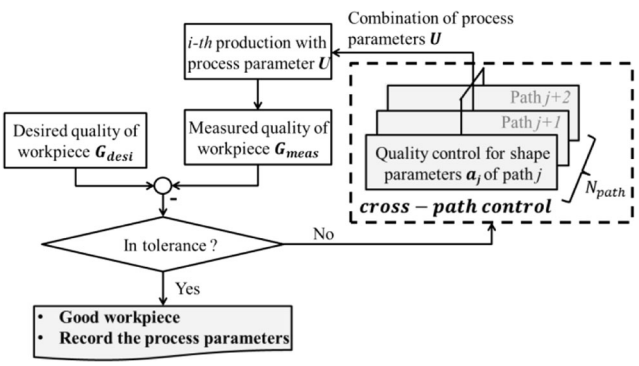

Fig. 3 Schematic flow chart of quality control for a LCM process chain

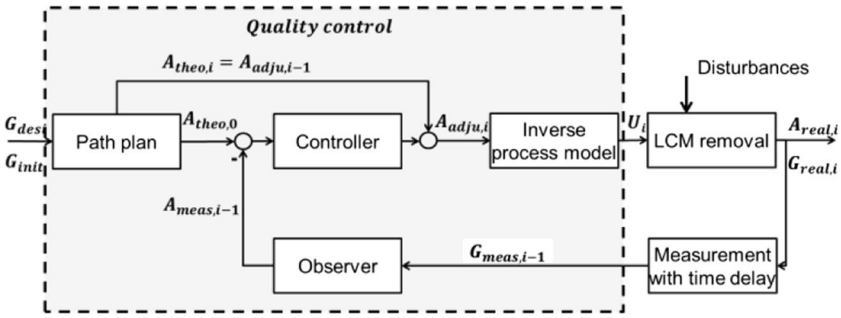

Fig. 4 LCM quality control with feed-forward modules

productions. In order to realize the control concept, the following challenges have to be overcome:

- The LCM is a multi-inputs-multi-outputs (MIMO) system.
- The relations between the process input parameters (actuating variables $\boldsymbol{u}$) and the shape parameters of one removal (control variables $\boldsymbol{a}$) are non-linear, and the probable shape parameters for a single removal as well as the respective process input parameters cover a wide range.
- The interactions between the LCM subsystems such as the mechanical positioning unit, the etchant pump, the laser source, and its optical system are not clear.
- The interactions between overlapping removal paths are partly unknown.

Details of how these challenges are met by a non-linear MIMO quality control system are provided in Section 4.

4 Design of the quality control

An inverse process model and a process chain prediction are the foundations of the feed-forward control. For this purpose, the shape parameters of the single removal and the geometry of the workpiece are characterized in Sections 4.1. Then, the required mathematical model for describing the relation between the shape parameters and the process input parameters as well as a process chain simulation with overlapping removal paths are presented in Sections 4.2 and 4.3, respectively. Both are finally combined with optimization algorithms to realize an inverse process model and a process chain prediction in Section 4.4.

Furthermore, the feedback loop consists of the post-production measurement that can be interpreted as a dead-time element, an observer for rebuilding the control variables from the measurements, and a discrete integral controller (I-controller) with adaptive gain to achieve stability over the entire operating range of the LCM. The observer and the controller are described in Sections 4.5 and 4.6, respectively. The complete resulting control system is summarized in Fig. 13.

4.1 Control variables

In case the set-values of the LCM process parameters are not changed along the material feed direction for a single path, the produced removal remains theoretically the same along the path. Thus, a removal geometry resulting from multiple paths oriented parallel to the material feed direction, has a constant cross-section in feed direction. In this case, the 3D–geometry can be simplified by a 2D contour across the feed direction. The LCM control system is developed to only control the quality features in the cross-section plane of a single path and the workpiece, respectively.

4.1.1 Quality features of single removal

A cross-section of a single removal path can be theoretically approximated by a Gaussian function [9] and, thus, characterized by the center position with the position parameter x_0 and by the two shape parameters $\boldsymbol{a} = (a_1 \quad a_2)$: the amplitude as removal depth a_1 and the standard deviation as removal width a_2.

In practice, a removal associated to different process parameters not always produces a Gaussian contour. The 3D measurements of the removal cavity associated to feed rate and laser power are shown in Fig. 5a, and their average cross-sections along the material feed direction are illustrated in Fig. 5b. As a result, the removal contour starts with a V-shape and changes to a U-shape and then to a W-shape with increasing feed rate and laser power. For the removal depicted in Fig. 5b.1 (V-shape), the cross-section mostly matches the Gaussian approximation. In Fig. 5b.2 (U-shape), however, the deviation between the measured contour and the theoretical approximation is increased. For the cases in Fig. 5b.3, b.4 (W-shape), the Gaussian approximation is not valid anymore. In order to describe the U-shape removal more precisely, the

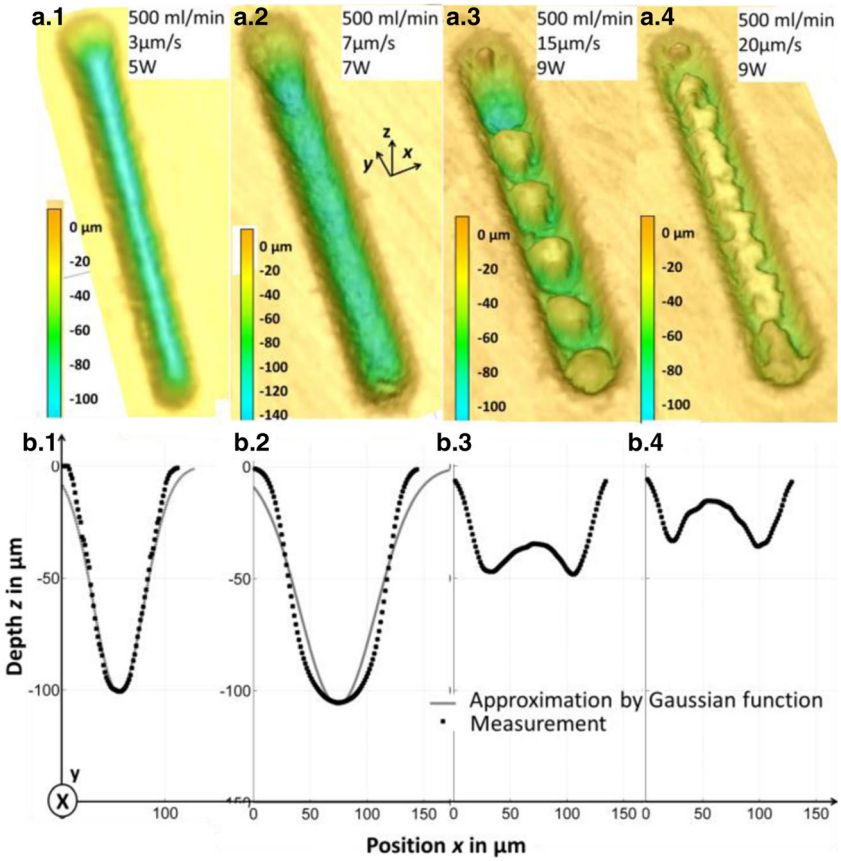

Fig. 5 Removal cavities associated to different process parameters: **a** 3D measurements by a confocal microscope Keyence VK-9710; **b** the average removal cross-section and its mathematical approximation for *b.1* and *b.2* using a Gaussian function

standard deviation of the Gaussian function is varied in relation to the position x and a deformation coefficient $\theta \in [0; 1]$ is introduced:

$$\boldsymbol{G}(a_1, a_2, x_0, \theta) = a_1 \cdot \exp\left(-\frac{1}{2} \cdot \left(\frac{x - x_0}{0.5 \cdot a_2 \cdot \Xi(\theta)}\right)^2\right),$$
$$\Xi(\theta) = \begin{cases} \frac{1-\theta}{\sigma} \cdot (x - x_0 + \sigma) + 1 & x \le x_0 \\ \frac{\theta - 1}{\sigma} \cdot (x - x_0 - \sigma) + 1 & x > x_0 \end{cases}. \quad (3)$$

By using this modified Gaussian function, the U-shape removal is sufficiently approximated, cf. Figure 6. Both the V-shape and the U-shape removals are stable and used for the LCM-production.

According to the experimental setup and the required temperature for a chemical reaction, the limits of the process parameters are $Q \in \left[300 \frac{\text{ml}}{\text{min}}; 500 \frac{\text{ml}}{\text{min}}\right]$, $\upsilon \in \left[3 \frac{\mu\text{m}}{\text{s}}; 20 \frac{\mu\text{m}}{\text{s}}\right]$, $P \in [3\ \text{W};\ 9\ \text{W}]$.

In addition, the upper limit of the laser power depending on the material feed rate for achieving either a V-shape or a U-shape removal is experimentally determined and illustrated as the curved upper surface in Fig. 7. The area between this upper surface and the lower plane defines the stable process window.

The resulting accessible shape parameters within these limits of the process parameters are shown in Fig. 8. These limits of the process parameters and of the removal shape for a single path are regarded as boundary conditions for the optimization when solving the inverse problem in Section 4.4.

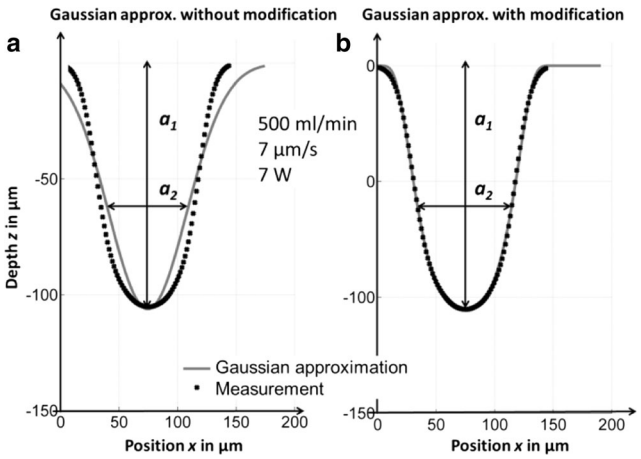

Fig. 6 Approximation of the removal cross section using a Gaussian curve and a modified Gaussian curve, respectively: **a** approximation by a Gaussian curve with $\theta = 1$; **b** approximation by a modified Gaussian curve with $\theta = 0.29$

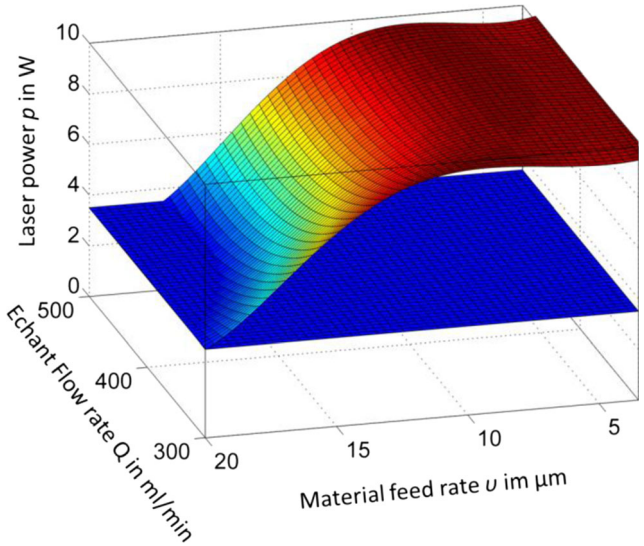

Fig. 7 Limits of process parameters for achieving a modified Gaussian removal by LCM

4.1.2 Quality features of a workpiece

The quality features of a workpiece are directly measurable, or calculated from the measured depth z along the position x. For example, the average depth d_{die} of a rectangular die can be calculated by an arithmetic mean of the measured depths z_m at the positions x_m at the bottom of the rectangular shape with M measuring points:

$$d_{\text{die}} = \frac{1}{M} \sum_{m=1}^{M} z_m. \tag{4}$$

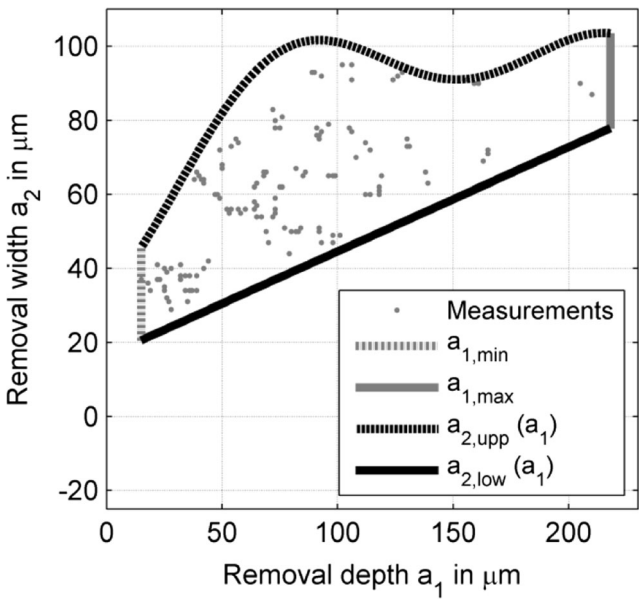

Fig. 8 Limits of the shape parameters for a single modified Gaussian removal: $a_{1,\text{min}}$: minimum of the removal depth; $a_{1,\text{max}}$: maximum of the removal depth; $a_{2,\text{upp}}$: upper limit of the removal width related to depth; $a_{2,\text{low}}$: lower limit of the removal width related to depth

Furthermore, the straightness S of the produced ground can be calculated by using a Chebyshev approximation [18]

$$S = \min_{c_1,\ c_2} \left\{ \lim_{n\to\infty} \sqrt[n]{\sum_{m=1}^{M} (e_m)^n} \right\}, \tag{5}$$

whereby $e_m = \frac{|c_1 \cdot x_m - z_m(x_m) + c_2|}{\sqrt{{c_1}^2 + 1}}$ is the orthogonal distance of the point $(x_m \quad z_m)$ to a linear geometry $z(x) = c_1 \cdot x + c_2$.

4.2 Process model

A quality control requires a model that describes the relations between the control variables and the actuating variables. Due to the partly unknown physical relations, analytical approaches for modeling the single removal are limited. For this reason, an artificial neural network using radial basis functions is used to describe the causality between the process input parameters and the shape parameters for a single removal [12]:

$$\boldsymbol{a} = \boldsymbol{H}_{\textbf{model}}(\boldsymbol{u}). \tag{6}$$

Note that $\boldsymbol{a} = (a_1 \quad a_2)$ and $\boldsymbol{u} = (P \quad v \quad Q)$.

As a result, an increased feed rate of the workpiece leads to a reduced removal depth, and higher laser power produces a deeper and wider removal. The flow rate of the etchant influences the removal rate on two sides. Increased flow rate causes higher reaction intensity, but also higher cooling speed in the processing area.

The deformation coefficient θ introduced in Eq. 3 can be uniquely determined by a defined removal depth a_1 and removal width a_2. The correlation is approximated with the polynomial function

$$\theta(a_1, a_2) = k_{00} + k_{10} \cdot a_1 + k_{01} \cdot a_2 + k_{20} \cdot {a_1}^2 + k_{11} \cdot a_1 \cdot a_2 + k_{02} \cdot {a_2}^2, \tag{7}$$

where the coefficients $k_{00} = 1.246$, $k_{10} = 0.006$, $k_{01} = -0.020$, $k_{20} = -5.002 \cdot 10^{-5}$, $k_{11} = 1.073 \cdot 10^{-4}$, and $k_{02} = -3.145 \cdot 10^{-5}$ are determined by a linear regression calculation. As a result, the number of degrees of freedom of the removal shape remains limited to two.

4.3 Simulation of process chain

Due to the distribution of thermal energy, the resulting geometry of the LCM process chain $\boldsymbol{G}_{\textbf{sim}}(\boldsymbol{A}, \boldsymbol{X}_0)$ with the shape parameters of multiple paths $\mathbf{A}$ and their

positions $\boldsymbol{X_0}$ can be simulated by a superposition of modified Gaussian curves

$$\begin{aligned} \boldsymbol{G}_{\mathbf{sim}}(x) &= \sum_{j=1}^{N_{\mathrm{path}}} \boldsymbol{G_j}(x), \\ \boldsymbol{G_j} &= \boldsymbol{G_j}(a_1, a_2, x_0, \theta(a_1, a_2)), \end{aligned} \tag{8}$$

whereby the single removal $\boldsymbol{G_j}$ is calculated according to Eqs. 3 and 7. With the simulation, the removal contour can be roughly estimated. However, the practical results usually do not match the simulation (cf. Figs. 11 and 14). Two major influences for this are

i. the angle-dependent influence on the flanks of the previous removal,
ii. the remaining thermal energy from the previous process.

To analyze both influences, a process chain with two overlapping paths is performed with the same process parameters. For solely investigating the influence (i.), an additional cooling path was implemented after the first removal at position $x_{0,1}$ and before the second removal path. The second path takes course parallel to the first one, and its middle position $x_{0,2}$ is located at the produced flank from the first path, so that the second removal is only influenced by the flank angle. For investigating the influence (ii.), the second removal was produced directly at the end of the first path in opposite direction to keep the remaining thermal energy. Its middle position is located at the edge of the overlapping area, so that the flank angle from the first path is close to 0° to obviate the effect of an angle-dependent influence on flanks. The trajectory plans and the feed direction of both experiments are drafted in Fig. 9.

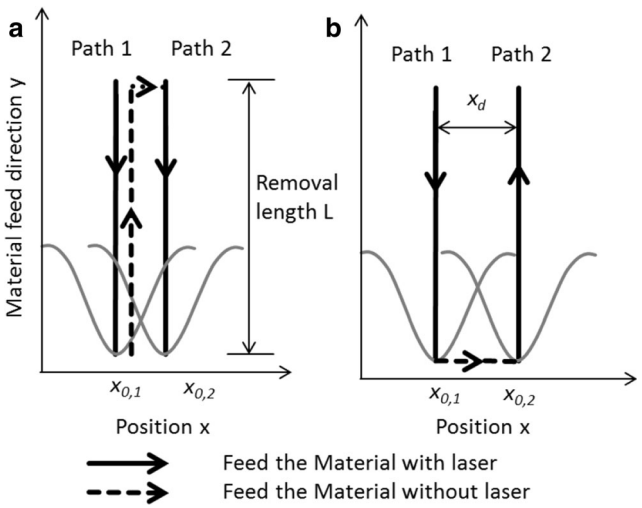

Fig. 9 Trajectory plan of removal paths in feed direction: **a** two overlapping paths in parallel direction to analyze the interaction resulting from the flank angle; **b** two paths in opposite direction to analyze the interaction resulting from remaining thermal energy. x_d refers to the distance between the middle positions x_0 of two paths

Figure 10 shows a simulated process chain with a superposition of two removals indicating the flank angle at the edge of the first path, where the middle position of the second path is located.

The comparison between the two experiments and the respective simulation results is presented in Fig. 11. The experimental results show that the flank angle (influence *i.*) causes a reduced removal depth of the second path with the negligible change of the width, see Fig. 11a. The remaining thermal energy influence (influence ii.) results in more material removal with an increased depth and width, see Fig. 11b.

In practice, the LCM removals are usually processed with the overlapping paths in the opposite direction, so that the processing time and energy efforts can be minimized, and a possible positioning deviation can be avoided. In this case, the removals are influenced by both flank angle and thermal energy. The two effects compensate each other partly. The remaining deviation from the path planning can be controlled with the developed quality control system.

4.4 Optimization with cost function

A feed-forward control requires inverse models. In the LCM quality control, an inverse LCM process model is used to obtain a direct access to the control variable. A further inverse process model is used for the path planning, which means planning the desired shape parameters and the positions of the multiple paths. Both blocks, cf. Fig. 13, can be provided by iterative optimizations of the forward model described in Sections 4.2 and 4.3. A minimal deviation between the simulated and the desired value is searched by using the least-squares method.

The function $\widetilde{\boldsymbol{IH}}_{\mathbf{model}}$ describes the inverse LCM process model for a single removal:

$$\boldsymbol{u} = \widetilde{\boldsymbol{IH}}_{\mathbf{model}}(\boldsymbol{a}). \tag{9}$$

The process parameters $\boldsymbol{u}$ to produce a defined shape $\boldsymbol{a}_{\mathbf{theo}}$ are calculated with the least-squares approach

$$\min_{\boldsymbol{u}} \left[\left(\boldsymbol{H}_{\mathbf{model}}(\boldsymbol{u}) - \boldsymbol{a}_{\mathbf{theo}} \right)^2 \right] \tag{10}$$

by adjusting the process parameters. The minimization is realized by using the MATLAB function "fmincon" and the boundary conditions from Fig. 7. In the same way, the simulation of the process chain is optimized:

$$\min_{\boldsymbol{A}, \boldsymbol{X_0}} \left[\left(\boldsymbol{G}_{\mathbf{desi}} - \boldsymbol{G}_{\mathbf{sim}}(\boldsymbol{A}, \boldsymbol{X_0}) \right)^2 \right], \tag{11}$$

$$\boldsymbol{A} = \begin{bmatrix} a_{1,1}, \cdots, a_{1,j}, \cdots, a_{1,N_{\mathrm{path}}} \\ a_{2,1}, \cdots, a_{2,j}, \cdots, a_{2,N_{\mathrm{path}}} \end{bmatrix}^T$$

$$\boldsymbol{X_0} = \left[x_{0,1}, \cdots, x_{0,j}, \cdots, x_{0,N_{\mathrm{path}}} \right]^T.$$

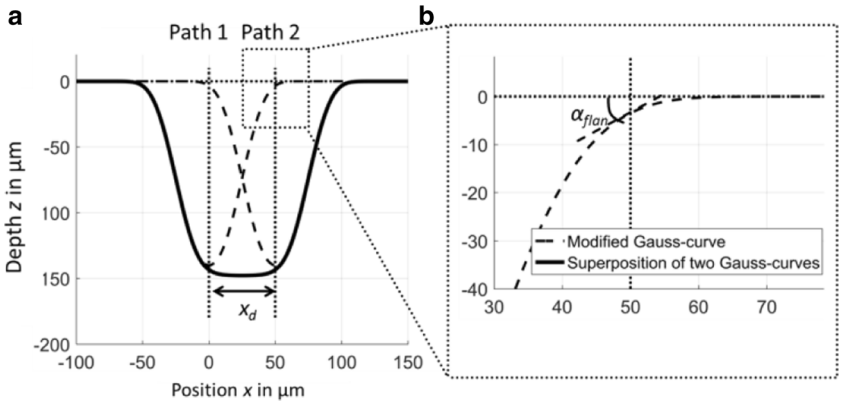

Fig. 10 Simulation of two overlapping paths with the distance x_d = 50 µm: **a** superposition of single removals; **b** flank angle of the first path at the middle position of the second path α_{flan} = 36°

The shape parameters and the position of each path are the degrees of freedom for minimization. They are limited by the conditions shown in Fig. 8 for a modified Gaussian removal.

4.5 Observer

The workpiece, produced by the path planning and its associated process parameters, is measured after each production. If the quality features of the workpiece exceed the tolerances, the process chain is required to be optimized by adjusting all the single removals. In this case, the non-measurable resulting shape parameters of the single paths are estimated by an observer according to the measured contour $\boldsymbol{G}_{\mathbf{meas}}$, so that they can be compared to the set-values from the path planning.

The approach of an observer is similar to the path planning. In order to rebuild the single removals reliably, the number of the degrees of freedom of the observer is usually less than for the path planning. For example, due to a small positioning deviation (<0.05 µm) caused by the linear stage, the center positions of the removal paths $\boldsymbol{X}_{\mathbf{0}}$ are assumed to be constant during the optimization, i.e.,

$$\min_{\boldsymbol{A}_{\mathbf{meas}}} \left[\left(\boldsymbol{G}_{\mathbf{meas}} - \boldsymbol{G}_{\mathbf{obse}}(\boldsymbol{A}_{\mathbf{meas}}, \boldsymbol{X}_{\mathbf{0}}) \right)^2 \right]. \tag{12}$$

Here, $\boldsymbol{G}_{\boldsymbol{obse}}$ results from a superposition of multiple modified Gaussian functions that are calculated with Eq. 3 using the estimated shape parameter $\boldsymbol{A}_{\mathbf{meas}}$.

4.6 Controller

According to the calculated shape deviations of every path in the previous production, the process parameters for the subsequent production are adapted by a quality controller.

A discrete I-controller with adaptive gain K, which is introduced in [19], is the suitable solution for this MIMO control system. With this controller, the set-value of the shape parameter for production i is calculated according to the previous set-value of the shape parameters $\boldsymbol{A}_{\mathbf{theo}}(i\text{-}1)$ and the shape deviations $\boldsymbol{E}(i\text{-}1)$:

$$\begin{aligned} \boldsymbol{A}_{\mathbf{adju}}(i) &= \boldsymbol{A}_{\mathbf{theo}}(i-1) + \boldsymbol{K}(i) \cdot \boldsymbol{E}(i-1), \\ \boldsymbol{E}(i-1) &= \boldsymbol{A}_{\mathbf{theo}}(0) - \boldsymbol{A}_{\mathbf{meas}}(i-1). \end{aligned} \tag{13}$$

In the LCM control, the non-linear LCM process is linearized by an inverse model. The resulting pseudo-linear system without consideration of interactions and disturbances reads

$$\boldsymbol{H}_{\mathbf{pseu}} = \widetilde{\boldsymbol{IH}}_{\mathbf{model}} \cdot \boldsymbol{H}_{\mathbf{LCM}} \approx 1. \tag{14}$$

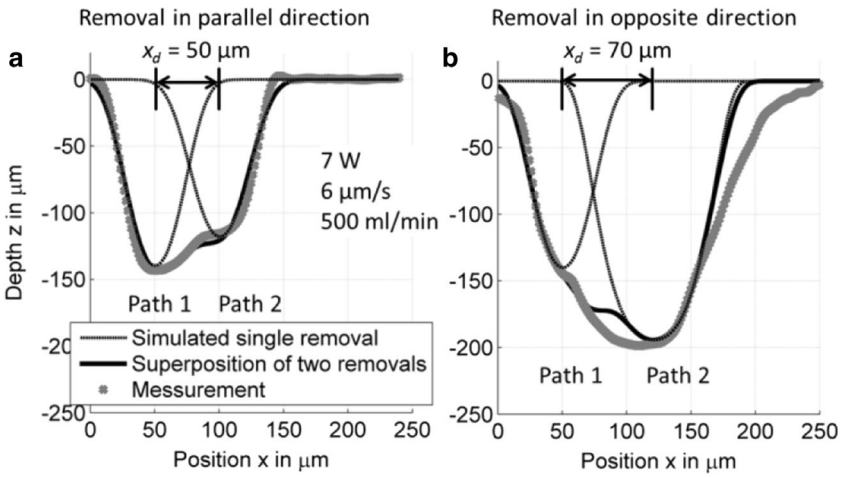

Fig. 11 Measurements of removal contours produced by two overlapping removals: **a** flank influence: removal in parallel with middle distance x_d = 50 µm and the theoretical flank angle α_{flan} = 36°; **b** influence of remaining thermal energy: removal in opposite direction with middle distance x_d = 70 µm and the theoretical flank angle α_{flan} = 0°

Furthermore, the relation

$$\boldsymbol{A}_{\mathbf{real}}(i) = \boldsymbol{H}_{\mathbf{pseu}}\left(\boldsymbol{A}_{\mathbf{adju}}(i)\right) \tag{15}$$

holds, cf. Fig. 13.

In order to determine the value of the gain K, there is a compromise between control speed and stability. A low value of K normally results in a stable system, but the control speed is slow. Based on experiments, the gain K is heuristically chosen to be $K = 1$. However, even for $K = 1$, the LCM process was not stable for certain operation conditions. As a result of the non-linearity of the LCM process, the control loop with a constant K cannot provide the stability and the satisfied control speed simultaneously in the whole operating area. In general, the operating area for a small removal contour is more sensible than for a larger one. And a large deviation between the set-value $\boldsymbol{a}_{\mathbf{theo}}$ and the measurement $\boldsymbol{a}_{\mathbf{meas}}$ requires a lower K. Therefore, an adaptive controller with the gain $\boldsymbol{K}(i)$, where i represents the number of the production step, is designed with the previous set-value of the shape parameters $\boldsymbol{A}_{\mathbf{theo}}(i\text{-}1)$ and the measured shape parameters $\boldsymbol{A}_{\mathbf{meas}}(i\text{-}1)$. This controller has different gains for each shape parameter in N_{path} processes $\boldsymbol{K}(i) = \begin{bmatrix} k_{1,1}, \cdots, k_{1,j}, \cdots, k_{1,N_{\mathrm{path}}} \\ k_{2,1}, \cdots, k_{2,j}, \cdots, k_{2,N_{\mathrm{path}}} \end{bmatrix}^T$, and its elements for the i-th production are calculated by

$$k_{n,j}(i) = \frac{\boldsymbol{A}_{\boldsymbol{n,j,theo}}(i\text{–}1)}{\boldsymbol{A}_{\boldsymbol{n,j,E}}(i\text{–}1) + \left|\boldsymbol{A}_{\boldsymbol{n,j,theo}}(i\text{–}1) - \boldsymbol{A}_{\boldsymbol{n,j,meas}}(i\text{–}1)\right|}, \tag{16}$$

respectively. In this case, k is close to 1 for a small deviation, and reduced for an increased deviation. Thus, a stable control system with a satisfied control speed is realized in the whole operating area.

This controller is verified by a simulated production. For the sake of simplicity, a single path production is considered here. It is assumed that the possible influence of the flank angle is simulated by an increased material feed rate $v + \Delta v$:

$$\boldsymbol{a}_{\mathbf{sim,flan}} = \boldsymbol{H}_{\mathbf{model}}(P \quad v + \Delta v \quad Q), \tag{17}$$

and an increased laser power $P + \Delta P$ produces the remaining thermal energy

$$\boldsymbol{a}_{\mathbf{sim,ther}} = \boldsymbol{H}_{\mathbf{model}}(P + \Delta P \quad v \quad Q). \tag{18}$$

Figure 12 shows an example of the shape parameters from a simulated removal during 10 production steps by using the adaptive controller and a controller with the constant gain $K = 1$. For this simulation, Eq. 18 was applied as LCM process model with $\Delta P = 2$ W. The control loop with the constant K has an oscillating output and is not stable, while the shape parameters reach the desired values at the fifth production by using the adaptive controller. Similar results are obtained

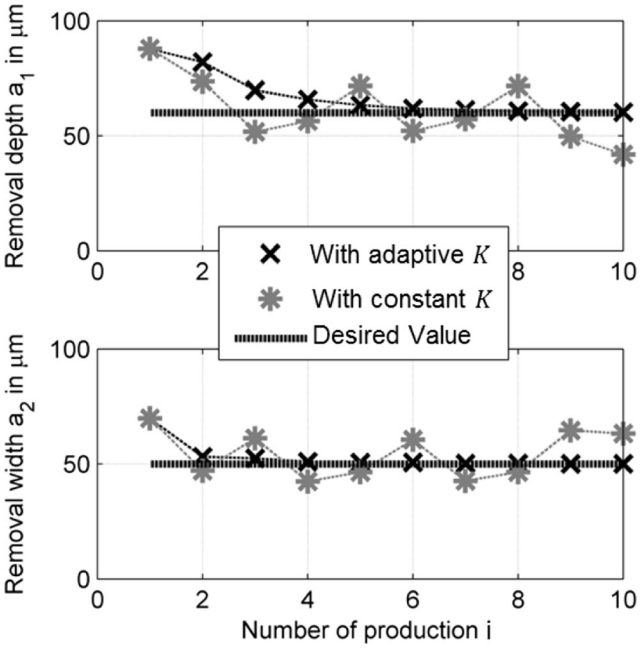

Fig. 12 Verification of the controller with a single path. Production: produced removal depth a_1 and width a_2 after production i. The set-values of the shape parameters are $a_1 = 60$ µm and $a_2 = 50$ µm. The LCM process is simulated with Eq. 18

when using Eq. 17 as LCM process model. As a result, the adaptive controller allows to compensate both influences, from the flank angle and the remaining thermal energy.

The resulting complete control concept with the path planning, the adaptive controller, the inverse process model and the observer is finally depicted in Fig. 13.

5 Validation and application

The developed quality control is validated by an application to produce a micro forming tool in the shape of a rectangular die. The quality features of this workpiece are the depth d_{die} and the straightness S of the produced ground surface in cross-section. They can be calculated by Eqs. 4 and 5. The tolerances of these quality features are defined to $\Delta d_{\mathrm{die}} = \pm 5$ µm, $S = 2$ µm.

The control variables are the shape parameters of four paths $\boldsymbol{A}$. The desired contour of the tools reads

$$\boldsymbol{G}_{\mathbf{desi}}(x) = \begin{cases} -D_{\mathrm{desi}}, & |x - x_c| < W_{\mathrm{desi}}/2 \\ 0, & \text{otherwise} \end{cases}, \tag{19}$$

i.e., a rectangular shape with the depth $D_{\mathrm{desi}} = 100$ µm and the width $W_{\mathrm{desi}} = 200$ µm at the center position $x_c = 200$ µm.

Within the process limits, this workpiece can be produced with four paths. Their center positions are

$$x_{0,j} = \frac{W_{\mathrm{desi}}}{2 \cdot N_{\mathrm{path}}} \cdot (2 \cdot j - 1). \tag{20}$$

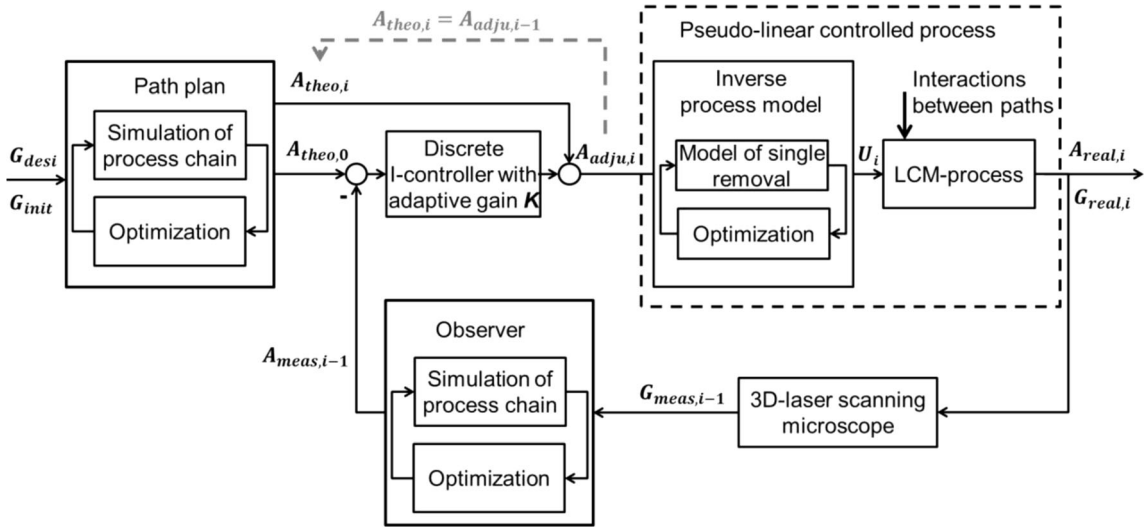

Fig. 13 The quality control concept with path plan, controller to adjust the shape parameters of the removal paths, inverse process model, and observer for LCM

The path plan to produce the rectangular die as well as the measurements of the produced contours for the subsequent production steps are shown in Fig. 14a, b, respectively. The 3D measurement of the finally obtained workpiece is presented in Fig. 15. The production of such a workpiece takes about 5 min.

In order to simplify the simulation of single removals, the paths affected by interactions, the path 2, 3, and 4, are set to the same removal width, and their middle positions are set to the initial location. As a result, the degrees of freedom of the 4 paths were reduced from 12 to 6:

$$\left(a_{1,1}\cdots a_{1,4}, a_{2,1}\cdots a_{2,4}, x_{0,1}\cdots x_{0,4}\right)\rightarrow\left(a_{1,1}\cdots a_{1,4}, a_{2,1}\cdots a_{2,4}\right).$$

By using Eq. 12, the single shape parameters of the measured contour $\boldsymbol{a}_{\mathbf{meas}}$ are simulated and compared to the desired values. Their deviations are led to the controller and used for optimizing the subsequent production. After two optimizations, a workpiece with satisfying quality features has been produced. The resulting depth $d_{\mathrm{die}} = 101.1$ μm and the straightness $S = 1.2$ μm of the achieved workpiece are obtained from the measured geometry according to Eqs. 4 and 5. The experimental results show that the maximal depth deviation of produced rectangular die from the desired value of 100 μm is reduced from 33.1 μm without closed-loop control to 10.3 μm after the first control loop and finally to a value of 2.4 μm within the tolerance after the second loop. As a result, the control system is stable and has a satisfying control speed.

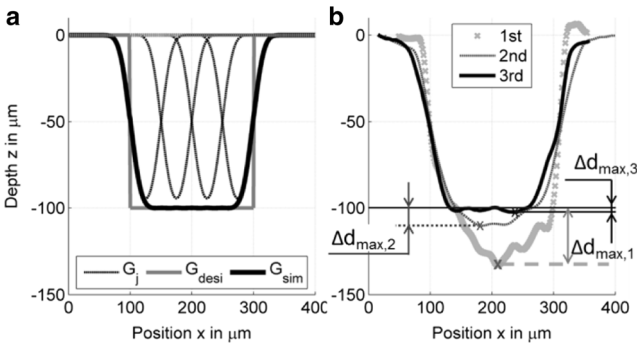

Fig. 14 Production of a rectangular die with four paths: **a** path plan; **b** cross-section of the produced workpiece for the first three optimization loops with the quality control system. The maximal depth deviation for the three productions are $\Delta d_{\max,1} = 33.1$ μm, $\Delta d_{\max,2} = 10.3$ μm, and $\Delta d_{\max,3} = 2.4$ μm

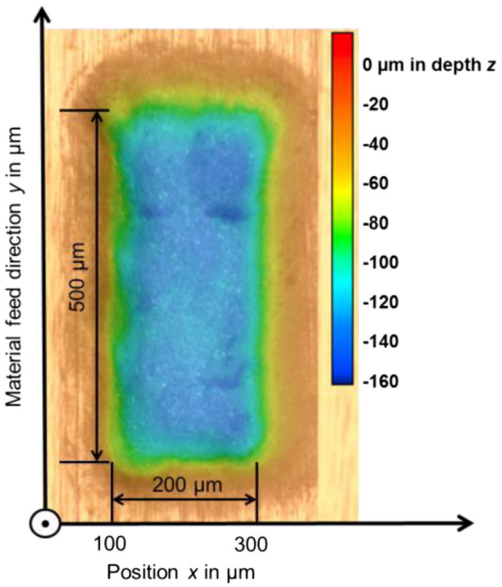

Fig. 15 3D–measurement of the produced rectangular die after three LCM productions, each with four subsequent paths

6 Summary

The shape parameters and positions of a sequence of LCM removals to achieve a desired geometry, as well as the process input parameters to produce the set-values of the shape parameters, are determined by using inverse models. The inverse models are realized by modeling the LCM process behavior using an artificial network approach and an iterative optimization algorithm. In the same way, the shape parameters resulting from single paths are derived from the post-process measured geometry using an observer. Based on the inverse models and an adaptive controller, a cross-path closed-loop quality control is developed for LCM. The adaptive controller is a discrete I-controller with adaptive gain for coping with the non-linearity of the LCM process and for providing a wide process operating range.

By using the proposed control system, a desired workpiece with a simple geometry, e.g., a rectangular die is obtained after several pre-productions. The number of pre-productions is normally less than 3, while it is more than 10 without the quality control, but with a manual adjusting. The resulting shape deviation from the desired shape amounts to 2.4 μm.

However, due to the reduced number of degrees of freedom, the reconstruction of single paths for a complex geometry is no more possible, e.g., for the production of an edge rounding by using multiple paths with different shape and position parameters. For this case, an in situ measurement is required to detect the temporary geometry after each removal. In addition, the post-process control system cannot compensate the random deviations along the material feed direction within one removal path. For this purpose, a real-time quality control with an in-process measurement has to be addressed in future works.

Acknowledgements The authors gratefully acknowledge the financial support by the Deutsche Forschungsgemeinschaft (DFG, German Research Foundation) for subproject A5 “Laserkontur” within the SFB 747 (Collaborative Research Center) “Mikrokaltumformen—Prozesse, Charakterisierung, Optimierung.”

References

1. Vollertsen F (2013) Micro metal forming. Springer, Heidelberg
2. Fulemova J, Janda Z (2014) Influence of the cutting edge radius and the cutting edge preparation on tool life and cutting forces at inserts with wiper geometry. Procedia Engineering 69:565–573
3. Lauwers B, Klocke F, Klink A, Tekkaya AE, Neugebauer R, Mcintosh D (2014) Hybrid processes in manufacturing. CIRP Ann Manuf Technol 63(2):561–583
4. De Silva AKM, Pajak PT, McGeough JA, Harrison DK (2011) Thermal effects in laser assisted jet electrochemical machining. CIRP Ann Manuf Technol 60:243–246
5. Pajak PT, De Silva AKM, Harrison DK, McGeough JA (2006) Precision and efficiency of laser assisted jet electrochemical machining. Precis Eng 30:288–298
6. Stephen A, Vollertsen F (2010) Mechanisms and processing limits in laser thermochemical machining. CIRP Ann Manuf Technol 59(1):251–254
7. Nowak R, Metev S (1996) Thermochemical laser etching of stainless steel and titanium in liquids. Applied physics A 63:133–138
8. Kray D, Fell A, Hopman S, Mayer K, Willeke GP, Glunz SW (2008) Laser Chemical Processing (LCP)—a versatile tool for microstructuring applications. Applied physics A 93:99–103
9. Mora A, Haase M, Rabbow T, Plath PJ (2005) Discrete model for laser driven etching and microstructuring of metallic surfaces. Phys Rev E 72(6):061604
10. Stephen A, Walther R, Vollertsen F (2009) Removal rate model for laser chemical micro etching. In: 5th International WLT-Conference on Lasers in Manufacturing (LIM), München pp 615–619
11. Mehrafsun S, Vollertsen F (2013) Disturbance of material removal in laser-chemical machining by emerging gas. CIRP Ann Manuf Technol 62:195–198
12. Zhang P, Goch G (2015) A quality controlled laser-chemical process for micro metal machining. Prod Eng 9(5):577–583
13. Uhlmann E, Mullany B, Biermann D, Rajurkar KP, Hausotte T, Brinksmeier E (2016) Process chains for high-precision components with micro-scale features. CIRP Ann Manuf Technol 65:549–572
14. Pfeifer T (2002) Quality management—strategies, methods, techniques. Carl Hanser, München
15. Goch G, Dijkman M (2009) Holonic quality control strategy for the process chain of bearing rings. CIRP Ann Manuf Technol 58(1): 433–436
16. Zhang P, Renken V, Goch G (2012) Cross-plane quality control concept of the bearing ring production. Mater Werkst 43(1–2):37–41
17. Grüne L, Pannek J (2011) Nonlinear model predictive control: theory and algorithms. Springer, London
18. Goch G, Lübke K (2008) Tschebyscheff approximation for the calculation of maximum inscribed/minimum circumscribed geometry elements and form deviations. CIRP Ann Manuf Technol 57(1):517–520
19. Lunze J (2010) Regelungstechnik 2-Mehrgrößensysteme, Digitale Regelung. Springer, Heidelberg, pp 518–525